Combined use of high-resolution dialysis, diffusive gradient in thin films (DGT) technique, and conventional methods to assess trace metals in reservoir sediments

Eyram Norgbey · Yiping Li · Ya Zhu · Amechi S. Nwankwegu · Robert Bofah-Buah · Linda Nuamah · Yashuai Pu

Journal: Environ Monit Assess

2020). Black water events negatively alter the beautiful appearances of reservoirs and cause a major income loss in the ecotourism industry because large sums of money are needed to rectify this issue. Black water events have been recorded in many water systems such as low-gradient rivers and reservoirs and are often associated with high amounts of organic matter (Duan et al., 2014). Dissolved oxygen is consumed during the decomposition of high organic matter in freshwater systems, making the water body hypoxic. The low oxygen concentration in the water system causes fishes and other aquatic organisms to die. Microbial decomposition of the dead aquatic species leaves the water system anoxic, creating favorable environmental conditions for the occurrence of black water events (Whitworth & Baldwin, 2016; Whitworth et al., 2013). In addition, variations of water temperature (thermal stratification) with depth due to local climate influence the oxygen distribution in reservoirs. Liu et al. (2019) demonstrated that high thermal stratification could cause the bottom water to be hypoxic, which affects the water quality of reservoirs. Iron plays a significant role in black water formation by reacting with organic matter (humic and fulvic acids) to produce black materials (Krachler et al., 2019). The hypoxic conditions at the water–sediment boundary (WSB) trigger the release of metals (iron (II), Fe^{2+}, and manganese (II), Mn^{2+}) from sediments, interacting with sulfide (S^{2-}) to produce black compounds made up of iron sulfide and manganese (II) sulfide (Rong et al., 2020). This indicates that WSBs are primarily responsible in the occurrence of black water events. Black water events have been recorded in several areas across the world, including Australia (Duval & Ludlam, 2001; Hladyz et al., 2011), China (Rong et al., 2020), Venezuela (Battin, 1998), the USA (Duval & Ludlam, 2001; Valett et al., 2005), and Finland (Berthon & Zibordi, 2010). Thus, it is significantly important to investigate black water formation to understand the mechanisms responsible for this phenomenon.

The structure of sediments is highly heterogeneous and complex; thus, they accumulate or discharge pollutants (trace metals) in the aquatic ecosystem (Xu et al., 2012). Trace metals affect microbial and plant growth and can cause cancer in humans, leading to death (Akoto et al., 2019). Trace metals come into the soil through anthropogenic sources such as mining, smelting, and fertilizer application (Jaishankar et al., 2014). Recent studies have demonstrated that under suitable conditions of DO (hypoxia), pH, and increasing redox potential, trace metals in sediments can easily migrate to the overlying water of the aquatic system. This can have dire consequences on the environment and pose a major threat to the public through water consumption (Yuan et al., 2020). In view of this, sediment quality guidelines (SQGs) were designed in past studies for the protection of water quality and aquatic ecosystems. It is important to note that SQGs measure the toxicity imposed on the aquatic environment by trace metals in sediment (Liao et al., 2017). Empirically derived SQGs, threshold effect level (TEL), and probable effect level (PEL) have been extensively used in recent works (Zhuang et al., 2019) to investigate trace metal toxicity in sediments. They have been used to reliably predict the toxicities of organic contaminants and trace metals in sediments without giving ambiguous results (Liao et al., 2017; Zhuang et al., 2019). The toxic effect is significant and occurs when metal concentrations are above the PEL values. However, the toxic effect is minimal when heavy metal concentrations are below TEL values. In this study, to understand the role trace metals play leading to the black water event, the toxicity of the trace metals in the Tianbao reservoir was evaluated at WSB using the SQGs.

Iron (Fe), manganese (Mn), phosphorus (P), and sulfur (S) are important nutrients that contribute positively to the aquatic ecosystem if in the right quantity. However, when available in high concentrations, these substances can also be hazardous to the aquatic system (Krueger et al., 2020). For example, Fe, a redox metal, is essential in the production of phytoplankton bloom and the oxidation process of organic matter in the aquatic environment (Li et al., 2020; Nwankwegu et al., 2020a). High Mn causes oxidative stress, which may lead to the death of aquatic organisms (Marks et al., 2017). P is a major contributor to algal blooms and eutrophication in the aquatic environment (Nwankwegu et al., 2020b). Large concentrations of sulfide (S^{2-}) are toxic to water organisms and the water environment (Shao et al., 2019). Thus, there is a need to understand the dynamics and availability of ferrous iron (Fe^{2+}), Mn^{2+}, S^{2-}, and soluble phosphate — PO_4^{3-} — in the sediments. Water bodies that experience black water events have an enormous amount of cations such as Mn^{2+} and Fe^{2+}, which combine with S^{2-}, contributing to its water quality deterioration (Rong et al., 2020). It is worth

noting that P also contributes to the formation of black water events (Li et al., 2020). For example, in Lake Taihu, P contributes significantly to the formation of algal bloom, which causes the so-called black blooms (black water) (Yan et al., 2019). Thus, it is important to understand the impact of Fe^{2+}, Mn^{2+}, S^{2-}, dissolved organic matter, and PO_4^{3-} in the aquatic sediments and to understand how they cause black water in southern China reservoirs.

Ex situ methods, which comprise sediment collection, treatment, and analysis, have been used to monitor metals and contaminants in sediments. These procedures do not accurately measure metal concentration due to disturbance of the sediment's physical and chemical properties during the transportation and laboratory process. Also, ex situ methods do not measure the dynamics of trace metals at the WSB (Xu et al., 2012). The thin film diffusive gradient (DGT) and high-resolution dialysis (high-resolution peeper) methods accurately measure the mobility and bioavailability of heavy (trace) metals at the WSB (Yuan et al., 2020). It is worth noting that no studies have been conducted to evaluate the mobility of Fe^{2+}, Mn^{2+}, S^{2-}, and PO_4^{3-} at WSB of the Tianbao reservoir to unravel the role they play leading to black water events. Thus, this study focused on analyzing the toxicities of trace metals and on investigating the diffusion fluxes of Fe^{2+}, Mn^{2+}, S^{2-}, and PO_4^{3-} in the reservoir sediments. The outcomes of this study would provide valuable insights that should complement freshwater quality management designs appropriately.

Methodology

Site description

The Tianbao (TB) reservoir with latitudes and longitudes of 22° 52′ 15.84″–22° 53′ 16.51″ N and 108° 13′ 31.33″–108° 14′ 9.37″ E, respectively, can be found in the southern part of China (Fig. 1). The variation in water depth of the reservoir is pictured in Fig. S1. The catchment area of the reservoir is about 50 km^2. Tianbao reservoir in southern China is the major source of water supply for the locals in many cities in southern China and contributes to China's GDP. The capacity of the reservoir is estimated to be 13.6 million m^3. The reservoir is used for farming (agriculture) and serves a source of water supply. Besides, the reservoir plays a vital role in flood control, tourism, and recreation (Li, 2019b). In-depth information of the study area can be found in our previous research (Li et al., 2021; Norgbey et al., 2021). The reservoir has an estimated average depth of 16 m and is surrounded mainly by *Eucalyptus* plantation.

Reservoir water properties (physiochemical)

The physical properties of the water (pH, oxygen, temperature, redox potential (ORP), turbidity, conductivity) for the Tianbao reservoir were measured from early March (spring) 2018 to February 2019 using the Yellow Springs Instruments (YSI) device (model name YSI EXO_2) obtained from YSI Company in the USA. These parameters were measured at sampling point A3 (deepest point in the reservoir) (Fig. 1) at 0.5-m intervals. The buoy (also located at sampling site A3) was stationed at the southeastern area of the reservoir (Fig. 1). The buoy was used to aid the YSI machine to telemetrically measure the physical parameters on-site. The buoy data for the above parameters were taken hourly in a day. For this research, the YSI data collected at 12 a.m. was interpreted because the thermal stratification is most steady during this period (Norgbey et al., 2021).

Water samples were collected in the various seasons in a year (winter, summer, spring, and autumn). We measured the manganese (Mn), sulfide (S), total iron (TFe), dissolved organic carbon (DOC), and total phosphorus (TP) concentrations in the water samples at the following sampling points: A1 to A4 (Fig. 1). The plexiglass water sampler, provided by Guangxi Water Research company, Nanning, was used to collect water in the following depths in the reservoir: 0.5 m, 3 m, 6 m, 9 m, 12 m, 15 m, and 18 m. The water storage container is made of polyethylene and has a capacity of 500 mL. For temporary storage of the water sample, 1.0 mL of nitric acid (HNO_3) was placed in the water samples that will be tested for total iron and manganese immediately after sampling. For sulfide, 1 mL of sodium hydroxide (NaOH) was placed in the water sample while 1 mL of sulfuric acid (H_2SO_4) was placed in the water sample for the determination of total phosphorus. For DOC, no chemical reagent was placed in

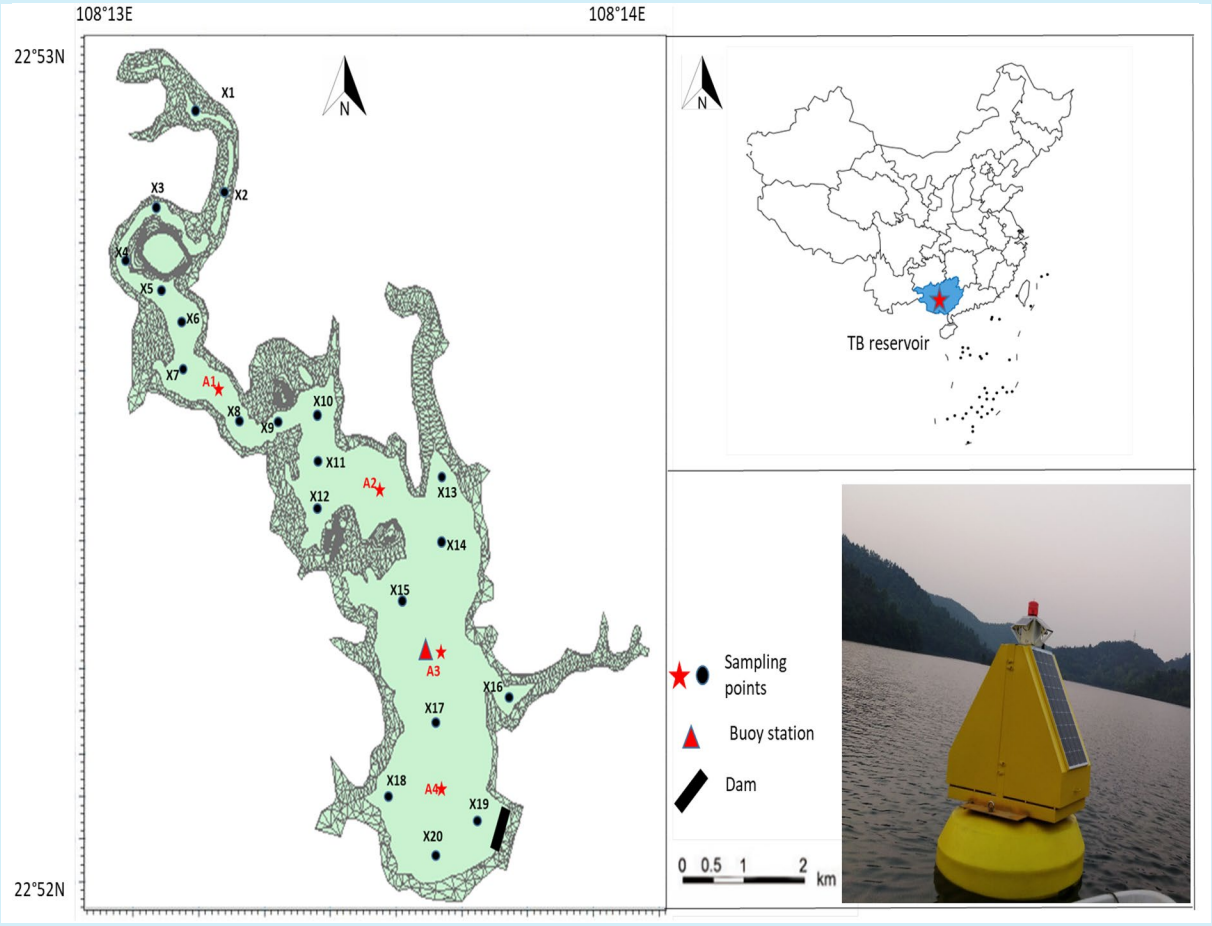

Fig. 1 Map of study area. A1, A2, A3, and A4 represent the four sampling points (using the core sampler) for the measurement of Fe^{2+}, Mn^{2+}, S^{2-}, PO_4^{3-}, and DOC in the sediment–water interface in the Tianbao reservoir. X1 to X20 represent the 20 sampling points (using the grab sampler) for the measurement of trace metals (Pb, Cu, Cd, Zn, and Ni) in the sediments. The variation in water temperature and dissolved oxygen were captured using the YSI device attached to the buoy station (A3)

the water samples. The water samples were stored at a temperature of 4 °C and transported to laboratory for testing. TFe and Mn were measured in the water samples with the help of inductively coupled plasma-optical emission spectrometry (ICP-OES; PerkinElmer Optima 8300, USA) (Li et al., 2021). TP was analyzed using the ammonium (NH_4^+) molybdate spectrophotometry method with the aid of a UV-1800 spectrophotometer, (Shimadzu, USA) (Shyla et al., 2011; Norgbey et al., 2021) while DOC was determined using the combustion oxidation method (non-dispersive) (Bisutti et al., 2004). Sulfide was analyzed in accordance with Norgbey et al.'s (2020b) procedure using methylene blue spectrophotometry.

Sediment sampling

Collection and sample analysis

Twenty surface sediments (Figs. 1, S1) were collected with a Van Veen grab sampler across the Tianbao reservoir in June 2018 for the evaluation of five trace metals (Pb, Cu, Cd, Zn, and Ni). The stainless steel grab sampler, with sample area and volume of 2500 cm^2 and 82 l, respectively, was provided to us by the Guangxi Water Research Company, Nanning, China. To prevent oxidation, the sediment samples were closed with cling film. The surface sediment samples (the whole grab sampler content) were stored

in closed plastic containers at 4 °C till laboratory testing. The freeze-dried sample was passed through a mesh made of plastic with an opening size of 0.15 mm. The sieved sample was microwave-digested (digestion time of 30 min and temperature of 150 °C) using an MLS-1200 MEG. The microwave-digested sample was mixed with concentrated nitric acid (HNO_3), hydrogen peroxide (H_2O_2), and hydrofluoric acid (HF) at a ratio of 3:1:1. The sample extract was filtered, and the trace metals (Pb, Cu, Cd, Zn, and Ni) in the filtrated solution were then tested in three replicates. The trace metals (Pb, Cu, Cd, Zn, and Ni) were determined using a Thermo Fisher Scientific instrument, an inductively coupled plasma mass spectrometer from the USA.

The sediment core sampler (UWITEC) was used for the collection of an undisturbed sediment core at A1, A2, A3, and A4 for the analysis of TFe, Mn, TP, and S^{2-}. The tube of the core sampler has a diameter of 90 mm. The core samples collected covered a depth of 25 cm. Sediment samples in the core sampler were divided into nine layers, namely 1 cm, 2 cm, 3 cm, 4 cm, 6 cm, 10 cm, 15 cm, 20 cm, and 25 cm. The sediment TFe was analyzed using an atomic absorption spectrophotometer (ICE 3000 Thermo Fisher Scientific, USA) while Mn was tested by aqua regia extraction-inductively coupled plasma mass spectrometry (Thermo Fisher Scientific, USA) (Melaku et al., 2005). For the total organic carbon (TOC) analysis, 1 M of hydrochloric acid (HCl) was added to the collected sediment to discard carbonates to measure TOC using a TOC analyzer machine (Aurora 1030C) (Yuan et al., 2020). Sediment TP was determined with X-ray fluorescence (XRF; Rigaku) in accordance with studies by Marip et al. (2020). The sulfide content was measured following past works (Rong et al., 2020) using ICP-OES (Thermo iCAP 6000). The detailed procedure for sulfide content measurement in the sediment is presented in supplementary sheet 1.

Quality assurance and quality control of trace metal assessment

Quality control (QC) of different trace metals was ensured by the computation of two spiked blanks and two method blanks. In this study, no trace metal was found in the blank samples. A high regression coefficient of calibration standards was obtained with a value of 0.99. The relative standard deviation (RSD) of the trace metals ranged from 2.1 to 4.9%, which guarantees reproducibility and precision. From matrix spiking experimental analysis, the percentage of recuperation of trace metal was from 80.1 to 115%. The soil reference materials (GSS-15) used in the analysis were collected from China Geophysical and Geochemical Exploration Institute.

Risk assessment

Q_{TEL} and Q_{PEL} represent the total risk quotients of the trace metals and are obtained according to Eqs. 1 and 2 (Zhang et al., 2017).

$$Q_{\mathrm{TEL}} = \sum_{.}^{\cdot}\left(\frac{C}{TEL}\right) \tag{1}$$

$$Q_{\mathrm{PEL}} = \sum_{.}^{\cdot}\left(\frac{C}{PEL}\right) \tag{2}$$

where C refers to the concentration of the trace metal in the sediment. If $Q_{PEL} > 1$, the trace metals in the sediment is defined as "toxic" while it is defined as "nontoxic" to benthic organisms if $Q_{TEL} < 1$. The risk is uncertain if $Q_{PEL} \leq 1 \leq Q_{TEL}$.

The initial assessments revealed that the concentrations of Pb, Cu, Cd, Zn, and Ni were relatively low. Thus, subsequent sampling at A1, A2, A3, and A4 focused on Fe, Mn, and P due to their relatively high concentrations in the sediment reservoir. The subsequent sample analysis was done using the high-resolution dialysis and diffusive gradients in thin film technique.

DGT and high-resolution peeper technique

Field sampling and device placement

The sediment core sampler (UWITEC) was used for the collection of an undisturbed sediment core at A1, A2, A3, and A4 (Fig. 1). The core sampler (UWITEC) was purchased from EasySensor Ltd., Nanjing, China. N_2 gas was pumped into the sediment cores to prevent it from oxidation. Also, it was covered with black materials to stop it from absorbing sunlight. The cores were moved to the laboratory for testing.

The Easy Sensor Institute, located in Nanjing, China, provided us with the DGT technology and high-resolution peeper sensor tools. The AgI thin film DGT was used to measure the S^{2-} content while the high-resolution peeper measured the metal ions (Fe^{2+}, Mn^{2+}, and PO_4^{3-}) and DOC in the WSB. The AgI DGT and high-resolution peeper can measure elements in the WSB with little disturbance. The high-resolution peeper was dipped in water without ions for a minimum of 16 h with nitrogen gas to get rid of unwanted oxygen. After 1 day of sample collection, the high-resolution peeper was introduced into the sediments for analysis. The high-resolution peeper's height in the overlying water was about 2.5 cm (Norgbey et al., 2020b). The high-resolution peeper system consists of 36 evenly spaced compartments filled with deionized water with each compartment having a volume of 400 µL. The high-resolution peeper works on the basis of the diffusion theory, where soluble elements travel through the permeable membrane (Xu et al., 2012). The content, determined by the high-resolution (HR) peeper, is the sediment pore water concentration (hypothetical) of the trace metals (Xu et al., 2012).

The AgI DGT devices were placed in a 0.01 NaCl solution and treated with nitrogen gas for 24 h to remove oxygen. Comprehensive information about the field sampling and placement of thin film diffusion gradient technology in sediments can be found at the original DGT manufacturer's website (www.dgt.research.com). A line was drawn on the DGT device to indicate the WSB before placing the device into the sediment samples. After 1 day (about 24 h) of placing the high-resolution peeper in the sediment samples, the thin film diffusion gradient technology device was placed into sediment (deployment time of 1 day). The devices were cleaned and then kept in a damp sealed container for further analysis. Similarly, after deployment of 48 h, the high-resolution peeper was thoroughly cleaned with a soft material to eliminate unwanted sediments (Norgbey et al., 2020b). In line with previous research, the thin film DGT and HR peeper device were brought to the laboratory for further examination (Xu et al., 2012).

Imaging and chemical analysis

The DGT-labile S in sediment samples was investigated using a computer image densitometry (CID) method with the binding gel scanned with a flatbed scanner at a resolution of 600 dpi (Xu et al., 2012). The content of $S^{2-}$was determined with thin film diffusion gradient technology (C_{DGT}) using Eq. 3.

$$C = \frac{M}{At} \tag{3}$$

where:

- M is the mass of element accumulated over the placement time
- t is the diffusion time (24 h)
- A is the area of each strip of the AgI DGT (cm^2)

For the high-resolution peeper, the cellulose membrane of peeper compartment sis perforated on each side, and the pore water is extracted and tested in the laboratory (Xu et al., 2012). PO_4^{3-}concentrations were calculated using the colorimetry molybdenum blue method (Murphy & Riley, 1962), and ferrous Fe (Fe^{2+}) concentration was tested using the colorimetric method of phenanthroline (Tamura et al., 1974). The content of Fe^{2+} in the pore water was acidized with HNO_3 to prevent Fe(II) oxidation (Yuan et al., 2020). Mn^{2+} concentration was measured according to studies by Soto-Neira et al. (2011) with the help of spectrophotometric technique. The photo-oxidation (UV) method of sequential injection spectrophotometry was used to determine DOC concentration in pore water (Tue-Ngeun et al., 2005). QC of dissolved Fe^{2+} and Mn^{2+} was ensured by the mensuration of standard solutions. A high relationship (correlation = $r > 0.8$) was measured. The standard deviation (elative) for dissolved Fe^{2+} is 4.7% while that of Mn^{2+} was 4.1%. Quality control of PO_4^{3-} was assured by measuring KH_2PO_4, which was the standard solution used. From test results, a strong relationship ($r^2 > 0.9$) was observed. The final analytical results were the mean of 3 replications to ensure precision and reproducibility. The mean RSD was 11%.

Apparent flux measurement at WSB

The apparent flux reveals both the magnitude and the diffusion direction of pollutants at the WSB. The apparent flux measured at the WSB was done using Eq. 4 (Zhang et al., 2020).

$$J = Jw + Js = -D_W(\frac{\partial C_.}{\partial X_W})_{(x=0)} \quad - \varphi D_S(\frac{\partial C_.}{\partial X_S})_{(x=0)} \tag{4}$$

where:

- J (g/(cm^2 s)) is the vector summation of Jw and Js
- Jw (g/(cm^2 s)) is fluxes of Fe^{2+}, Mn^{2+}, S^{2-}, and PO_4^{3-} from the benthic water to the sediment
- Js (g/(cm^2 s)) is fluxes of Fe^{2+}, Mn^{2+}, S^{2-}, and PO_4^{3-} from the sediment to the overlying water
- Φ is the sediment porosity
- $(\frac{\partial C_.}{\partial X_W})_{(x=0)}$ is the overlying water's concentration gradients
- $(\frac{\partial C_.}{\partial X_S})_{(x=0)}$ is the sediment's concentration gradients
- Dw (cm^2/s) is overlying water's diffusion coefficients of metals
- Ds (cm^2/s) is sediment's diffusion coefficients of metals

Porosity was determined from Eq. 5.

$$\Phi = \frac{Wd_s}{(1-W)d_w + Wd_s} \tag{5}$$

where:

- W is the water content determined via mass
- d_s is the sediment's mean density
- d_w is the overlying water's mean density

Data analysis

The experimental data was analyzed using Microsoft Excel 2016 (Microsoft company, USA) and the Origin 9.0 software. The site location was drawn using the ArcGIS 10.2 software (ENVI company, USA). Descriptive analysis and correlations were performed in Microsoft Excel 2016. One-way analysis of variance was used to evaluate the significant difference in this research in Excel Analysis ToolPak. p-values above 0.05 were deemed statistically irrelevant. Significant differences were identified when $p < 0.05$ (Huang et al., 2017, 2019; Norgbey et al., 2020a).

Results and discussion

Physiochemical water property of reservoir

The water quality properties (DO, water temperature, pH, Eh, and conductivity) of the reservoir were recorded from March 2018 to February 2019 at sampling point A3 (deepest sampling point). The changes in reservoir water temperature and DO concentration with reservoir depth are presented in Fig. 2 while the variation of pH and ORP with reservoir depth can be seen in Fig.S3. The conductivity of the reservoir water with depth for the sampling period is presented in Fig. S2. The findings indicate that thermal stratification was intense (strong) for the whole year with the exception of the months of December to January. From December to January, the reservoir water is completely mixed since the reservoir thermal structure is destroyed (Liu et al., 2019). Figure 2 reveals that the DO concentration of the benthic water in the reservoir was less than 2 mg/L from mid-April to late November 2018, leaving the benthic water hypoxic. The hypoxic benthic water during this period promoted redox reactions to take place at the benthic water. The mixing period of the reservoir occurred from December 2018 to January 2019, making the benthic water aerobic (Liu et al., 2019). The benthic water recorded a pH of 7.4–8.3 from January to July (weakly alkaline) while 6.5–7 (slightly acidic) was measured from August to December (Fig. S3). The ORP values at the benthic water were negative from September to November.

Figure 3 shows the seasonal changes with a water depth of TFe, Mn, sulfide, TP, and DOC in the reservoir water at A3. Similarly, the concentrations of total iron, manganese, sulfide, total phosphorus, and DOC at sampling points A1, A2, and A4 for spring (March), summer (July), autumn (October), and winter (December) are also presented in Table S1. The average amount of TFe in the benthic water (A3) in spring (March), summer (July), autumn (October), and winter (December) measured in milligrams/liter was 0.091, 0.11, 0.16, and 0.48, respectively. Similarly, the mean contents of Mn during the four seasons measured in milligrams/liter were 0.14, 0.04, 0.40, and 1.20, respectively, while those of S were 0.04, 0.02, 0.008, and 0.013,

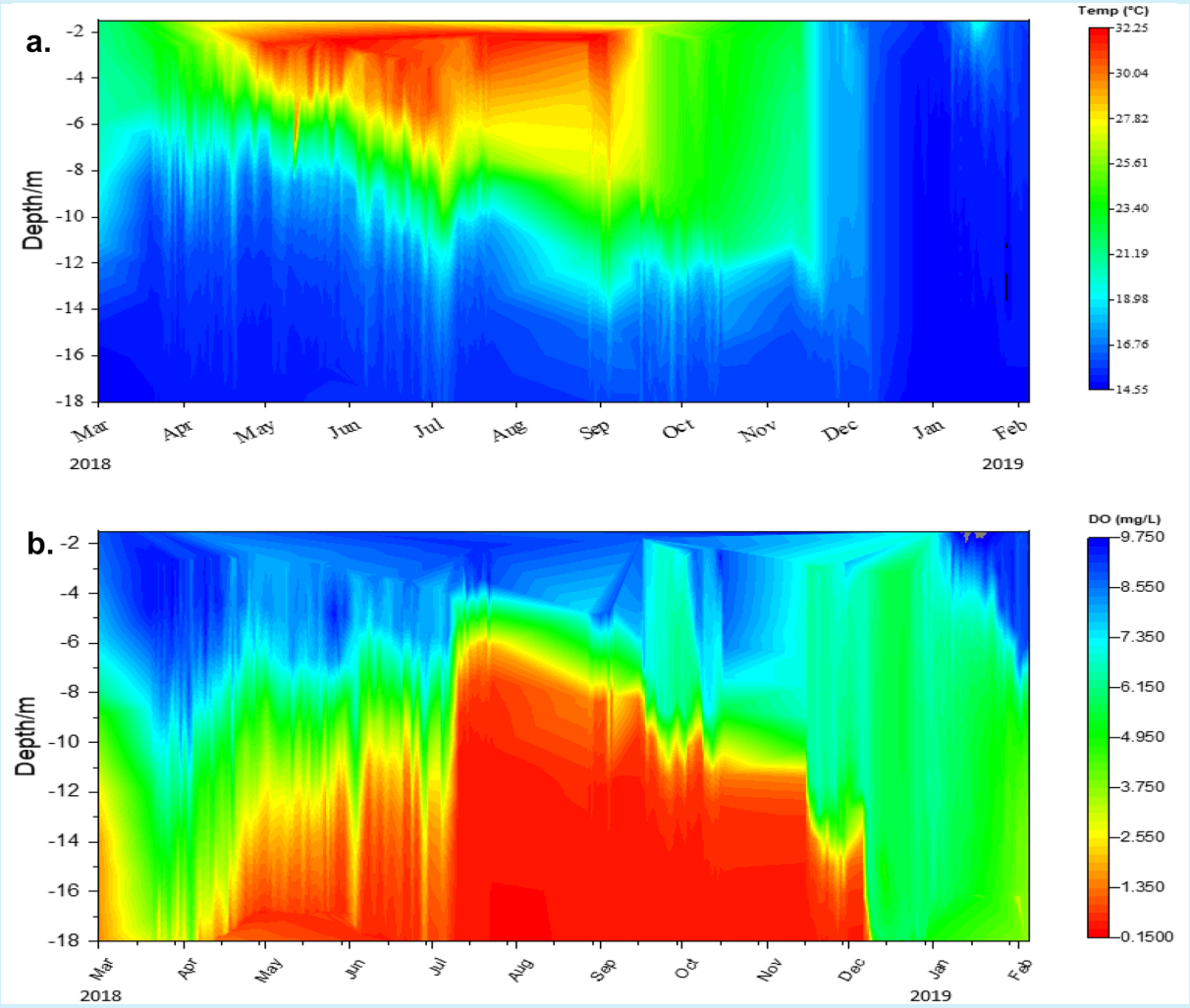

Fig. 2 Vertical distribution of **a** temperature and **b** dissolved oxygen in the reservoir from March 2018 to February 2019 at sampling point A3. Sampling data profiles were measured at 12 a.m. each day in the reservoir (depth = 18 m)

respectively. The average content of TFe and Mn in the benthic water significantly increased by 326% and 544%, while S reduced by 44.9%, respectively, from the mixing period in winter (high DO concentration) to the stratified period in summer (low DO concentration). The mean TP content in the benthic water (A3) measured in milligrams/liter was 0.017, 0.023, 0.033, and 0.077 while the DOC content was 2.1, 4.2, 20, and 18 mg/L for spring (March), summer (July), autumn (October), and winter (December), respectively. TP reported a spike of 215% from the mixing period in winter (high DO concentration) to the stratified period in summer (low DO concentration). Studies by Krueger et al. (2020) have shown that a hypoxic environment significantly enhances the reduction and decomposition of Fe^{3+} to Fe^{2+} and Mn^{4+} to Mn^{2+}. The hypoxic conditions at the WSB trigger microorganisms to use alternate electron acceptors such as Fe^{3+}, Mn^{4+}, and sulfate to oxidized organic matter. This triggers the release of metals (iron (II), Fe^{2+}, and manganese (II), Mn^{2+}) from sediments to the benthic water (Rong et al., 2020). In this work, the concentrations of TFe, Mn, and TP in benthic water increased substantially ($p < 0.05$) from the mixing period in winter (high DO concentration) to the stratified period in summer (low DO concentration), which strongly suggests that hypoxia promoted the discharge of

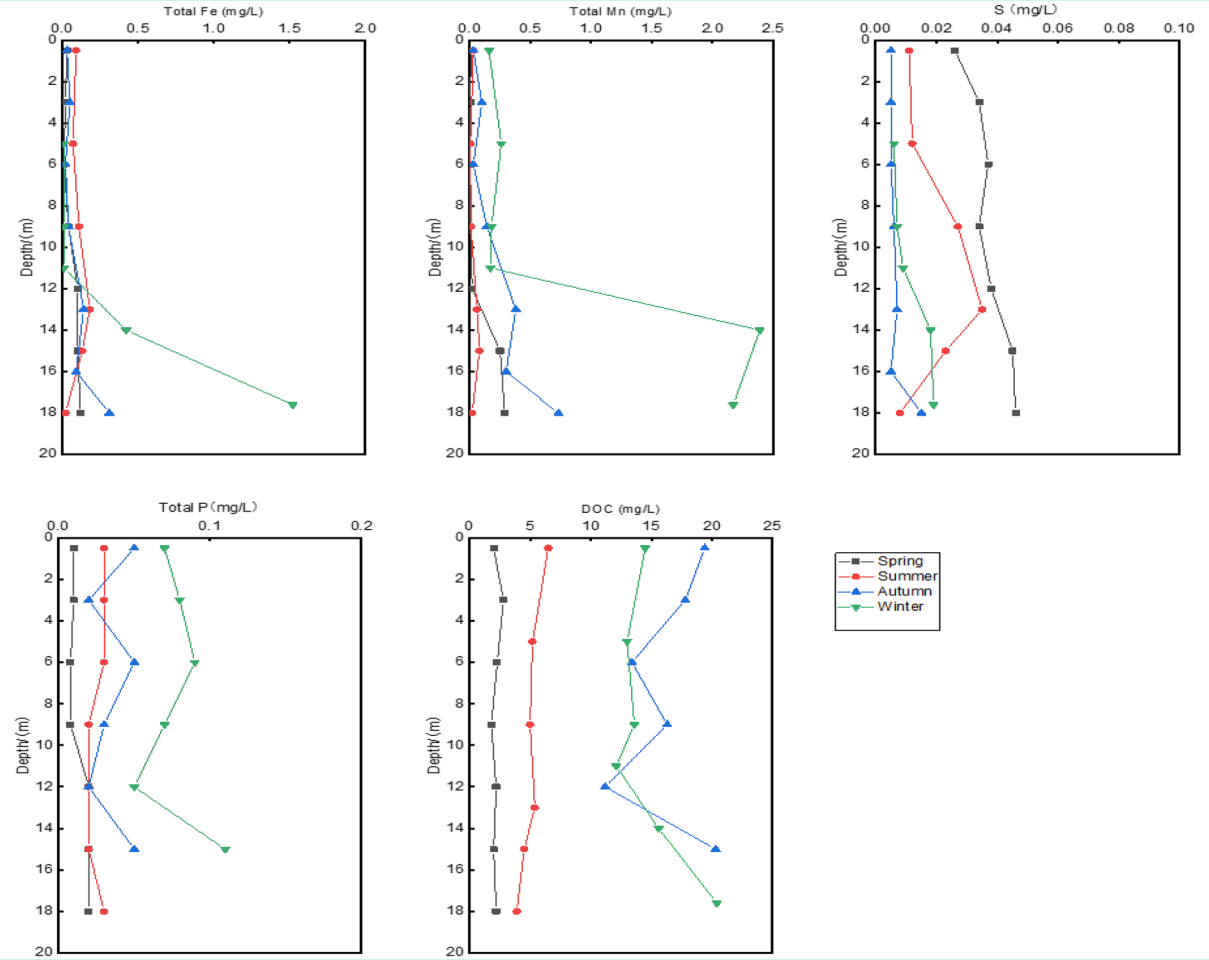

Fig. 3 Variations in the concentration of total iron (Fe), manganese (Mn), sulfide (S), total phosphorus (TP), and dissolved organic carbon (DOC) with water depth in the four seasons in the year at sampling point A3. For the variation in the concentration of Fe, Mn, and S with water depth for sampling sites A1, A2, and A4, please refer to Table S1

Fe-bound P and manganese from the reservoir sediments onto the benthic water (Luo et al., 2020).

Trace metal assessment in the sediments

The concentrations of the 5 trace metals (Pb, Cu, Cd, Zn, and Ni) in the sediments of the Tianbao reservoir were determined and compared with the values of TELs and PELs, as shown in Table 1 (Zhang et al., 2017). The concentrations of Pb, Cu, Cd, Zn, and Ni in the 20 sediment samples across the Tianbao reservoir were in the ranges of 10.7–72.8, 9.2–46.7, 0.10–0.50, 26.7–128.5, and 6.9–54 mg/kg dry weight, respectively (Figs. 1, S1). Pb, Cu, Cd, Zn, and Ni recorded mean (arithmetic) concentrations of 38.3, 29.9, 0.3, 84.6, and 22 mg/kg, respectively. The mean (arithmetic) values were almost similar to the median concentrations except for that of Zn. Ni, Pb, Cu, and Cd had lower mean and median concentrations when compared to their TELs (Table 1). The mean concentration Zn in most of the samples had values between its TELs and PELs. It is important to note that the concentration of Cd in all samples was lower than its TEL, while Zn had the least number of samples with their concentrations less than TELs. As for Pb, two-fifths of the samples had their concentrations between its TEL and PEL and three-fifths lower than its TEL. Similarly, Zn had two-fifths of the sample concentrations lower than its TEL and about three-fifths between its TEL and PEL. In this study, no sample

Table 1 Concentration of trace metals (Pb, Cu, Cd, Zn, and Ni) in the sediments (20 sampling points) of Tianbao reservoir. Sampling was conducted in June 2018 when thermal stratification of the reservoir was most intense

Metal	Arithmetic mean	TEL	PEL	SD	Max	Min	Geometric mean	Median	Number of samples			Total
									< TEL	TEL-PEL	> PEL	
Ni (mg/kg)	22.0	31.4	76.9	13.4	54.0	6.9	18.5	18.5	17	3	0	20
Cu (mg/kg)	29.9	45.5	181	15.3	46.7	9.2	25.9	26.5	14	6	0	20
Zn (mg/kg)	84.6	74.9	403	34.3	128.5	26.7	76.1	90.4	8	12	0	20
Cd (mg/kg)	0.30	3.0	18.9	0.20	0.50	0.10	0.20	0.2	20	0	0	20
Pb (mg/kg)	38.3	47.3	204	20.7	72.8	10.7	32.3	32.8	12	8	0	20
	Arithmetic mean	BSV		SD	Max	Min	Geometric mean	Median	> BSV			Total
Fe (g/kg)	40.7	ND		8.6	61.4	20.9	22.9	39.4	ND			17
Mn (g/kg)	0.7	0.181		0.2	1.2	0.4	0.8	08	17			17

TEL threshold effect level, *PEL* probable effect level, *SD* standard deviation, *BSV* background soil value

exceeded its PEL value. In general, the majority of the concentrations of Pb, Cu, Cd, Zn, and Ni (trace metals) were lower than the corresponding TELs, while others in the Tianbao reservoir sediments were between their TELs and PELs. The toxicity of trace metals (Pb, Cu, Cd, Zn, and Ni) on the environment was investigated using the total risk quotients based on Q_{PEL}. The total toxicological risks from each trace metal (i.e., $\frac{Qipel}{Qpel}$) in the Tianbao reservoir is shown in Fig. 4. From the 20 samples (Figs. 1, S1), the $Q_{i,PEL}$ of Pb, Cu, Cd, Zn, and Ni contributed to 12–29%, 12–26%, 0.8–2.4%, 15–55%, and 20–44% of Q_{PEL}, respectively. The results indicated that Zn and Ni made the major contribution of trace metal toxicity on the sediments. This was followed by Cu ≈ Pb, with Cd making the least contribution. Overall, the concentrations of the five trace metals (Pb, Cu, Cd, Zn, and Ni) were low, showing that the sediments in the Tianbao reservoir had limited harmful effects on the aquatic environment. The TOC content with the

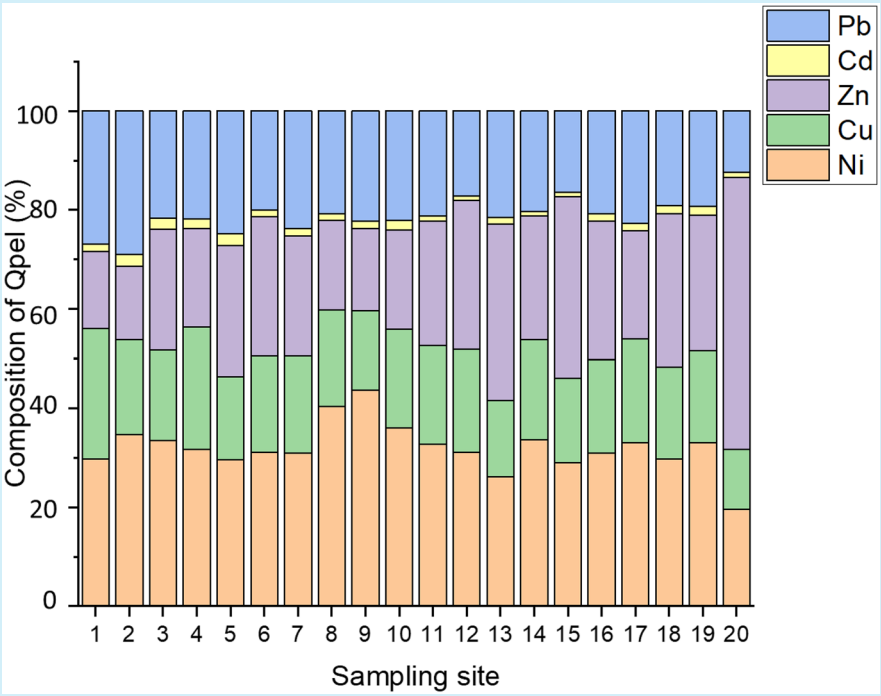

Fig. 4 Contributions of five trace metals (Pb, Cu, Cd, Zn, and Ni) to the total risk quotients (Q_{PEL}) of sediments of Tianbao reservoir

sediments ranged from 2.7 to 8.2%. The difference in TOC concentration at A1 to A4 was insignificant, with a p-value greater than 0.05 (Table S2). The high amount of TFe and Mn measured in the Tianbao reservoir (Table 1) were similar to our previous studies (Li et al., 2018). The average Mn values were about 4 times bigger than the soil background value (SBV) of Mn in Tianbao (Cheng et al., 2014). TFe and Mn concentrations in the sediment samples in the Tianbao reservoir were in the range of 20.9–61.4 and 0.4–1.2 g/kg dry weight, respectively. The arithmetic and geometric mean concentrations of Mn were 0.7 and 0.8 g/kg, respectively, while those of Fe were 40.7 and 22.9 g/kg, respectively (Table 1). All the Mn concentrations recorded in the sediments were substantially greater than their respective SBV. The total concentrations of TFe, Mn, S, and P in sediments (0–20 cm) from the sampling points (A1 to A4) ranged from 4000 to 80,000 mg/kg, 16 to 1900 mg/kg, 0.74 to 29 mg/kg, and 100 to 700 mg/kg, respectively, with an average of 33,000 mg/kg, 690 mg/kg, 9.1 mg/kg, and 490 mg/kg, respectively (Fig. S4). These results clearly show that the average values of TFe, Mn, and P were significantly bigger than the SBV recorded in Nanning, China. Studies by Cheng et al. (2014) recorded 5.32 mg/kg, 181 mg/kg, and 305 mg/kg as the background soil values for TFe, Mn, and P, respectively. The high concentration levels of TFe, Mn, and P at the sampling sites compared to the SBV in Nanning (Cheng et al., 2014) are likely due to a large number of human activities (industries, farming, and construction works) around the reservoir.

Anthropogenic activities in this region include the manufacture of steel and iron alloys, production of batteries, fireworks, mining activities, and glassware manufacturing, which are major sources of trace metal pollution (Deng et al., 2020; He et al., 2020; Zhuang et al., 2019). Also, rapid urban development also contributed significantly to trace metal pollution (Deng et al., 2020; Huang et al., 2015). The pollutants (Fe, Mn, and P) are transported due to stormwater runoff from these sites to the reservoir (Deng et al., 2020; He et al., 2020; Zhuang et al., 2019). Our results indicate that Fe, Mn, and P were stockpiled in the sediments (Xu et al., 2012). The observed accumulation of high concentrations of TFe, Mn, and P in the reservoir sediments was consistent with previous studies in this region (Deng et al., 2020; He et al., 2020; Zhuang et al., 2019). Due to the high concentration of TFe, Mn, and P in the reservoir sediments, the high-resolution peeper was employed to study the concentration, dynamics, and flux of Mn, P, and Fe while DGT examined that of sulfide at the WSB.

Dynamics of Fe^{2+}, Mn^{2+}, S^{2-}, PO_4^{3-}, and DOC at WSB using high-resolution peeper and DGT

The high-resolution peeper and the DGT device (having a high spatial resolution) were used in this study to elucidate the variation, availability, and mobility of Fe^{2+}, Mn^{2+}, S^{2-}, PO_4^{3-}, and DOC at the WSB (Zhang et al., 2019). Figure 5 shows the vertical distribution of Fe^{2+}, Mn^{2+}, S^{2-}, PO_4^{3-}, and DOC at A1 to A4 while Fig. S5 shows the 2-D image profiles of S^{2-} at the WSB. The concentrations (measured in mg/L) ranged 0.4–30, 0.2–11, 0.012–0.035, 0.030–0.60, and 5.6–54.9% for Fe^{2+}, Mn^{2+}, S^{2-}, PO_4^{3-}, and DOC, respectively, at the sampling areas. The mean content (measured in mg/L) of labile Fe, Mn, S, P, and DOC at the overlying water was 2.7, 4.6, 0.017, and 0.10 mg/L and 16%, respectively, while those for the sediments were 11.4, 7.5, 0.023, 0.2, and 35.9% respectively, for all sampling sites. Overall, the concentrations of Fe^{2+}, Mn^{2+}, S^{2-}, PO_4^{3-}, and DOC were larger in the sediments than in overlying water (Fig. 5). The difference in the concentration of Fe^{2+}, Mn^{2+}, PO_4^{3-}, and DOC between overlying water and sediments was significant ($p < 0.05$) while that of C_{DGT}–S was insignificant. A high correlation ($p < 0.05$) was recorded for Fe–DOC, Fe–S, and Mn–S at A3 with values of 0.9, 0.8, and 0.7, respectively (Table 2). For A2, the correlations of Fe–DOC, Fe–S, Fe–P, and Mn–S ($r \geq 0.7$, $p < 0.05$) were significantly high. On the other hand, the correlations at A1 for Fe–DOC, Fe–S, Fe–P, and Mn–S ($r \geq 0.2$, $p < 0.05$) were relatively low. For A4, the correlation for Fe–DOC, Fe–S, Fe–P, and Mn–S were positive with values of 0.9, 0.3, 0.7, and 0.4, respectively.

The transformations in the chemical state of Fe, Mn, P, and S at the WSB are influenced by many conditions such hypoxia (low oxygen concentration), presence of organic matter, low ORP, and the nature of sediments (Yuan et al., 2020). In this study, the TOC was measured at the hypoxic WSB of the sampling sites (A1 to A4) (Table S1). The presence of TOC at these points was due to the availability of a *Eucalyptus* plantation surrounding the reservoir.

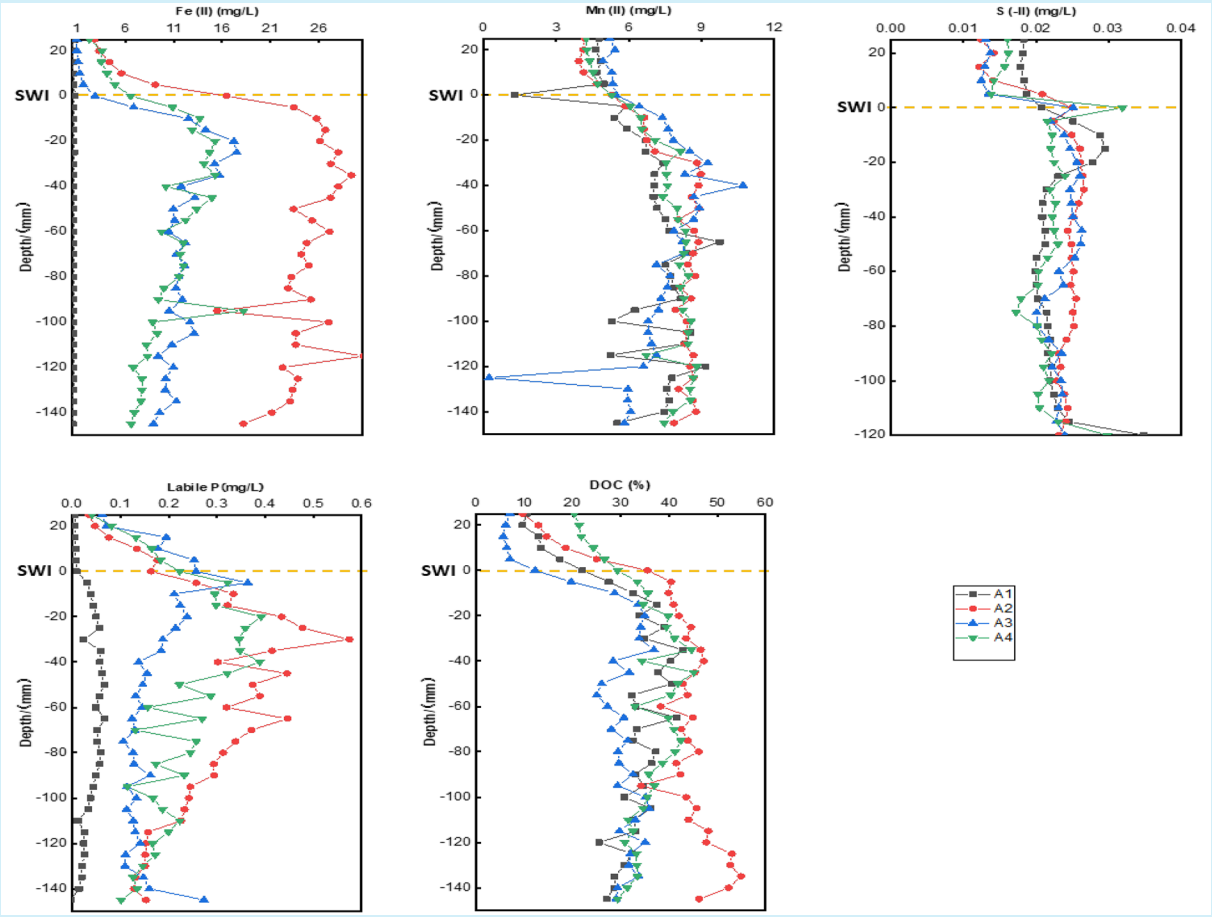

Fig. 5 Variation of Fe^{2+}, Mn^{2+}, S^{2-}, PO_4^{3-}, and DOC in sediment-overlying water profiles (A1–A4) in the Tianbao reservoir. The concentration of S^{2-} (one dimension) was computed from the mean values from the two-dimensional images presented in Fig. S4 (SWI sediment–water interface)

The organic residues (leaves) of the trees were transported into the reservoir via rainfall and wind during the rainy seasons (June to July) (Luo et al., 2020).

Table 2 Pearson correlation between Fe–S, Mn–S, Fe–P, and Fe–DOC at sampling sites A1, A2, A3, and A4 of Tianbao reservoir

r	A1	A2	A3	A4
Fe–S	0.23*	0.90*	0.83*	0.34*
Mn–S	0.21*	0.78*	0.75*	0.41*
Fe–P	0.34*	0.67*	−0.01*	0.67*
Fe–DOC	0.38*	0.87*	0.94*	0.88*

*Significantly different when comparison was done between Fe–S, Mn–S, Fe–P, and Fe–DOC at sampling sites A1, A2, A3, and A4 ($p < 0.05$, confidence interval 95%, descriptive statistics; $a = 0.05$, one-way ANOVA)

During the oxidation of organic matter in the hypoxic environment setting where the ORP value is low, microorganisms play a major role in converting Fe^{3+}, Mn^{4+}, and sulfate to Fe^{2+}, Mn^{2+}, and S^{2-}, respectively. These microorganisms use alternate electron acceptors such as Fe^{3+}, Mn^{4+}, and sulfate to oxidize organic matter. This oxidation process of organic matter also causes the release of PO_4^{3-} located within the organic material (Rong et al., 2020). Research works by Rong et al. (2020) also implied that iron-reducing bacteria contribute to the reduction of Fe^{3+} in WSB during hypoxia when the concentration of Fe^{2+} is significantly higher than that of S^{2-}. In this study, the concentrations of Fe^{2+} at A1, A2, A3, and A4 were significantly higher ($p < 0.05$) than those of S^{2-}. This suggests that iron-reducing bacteria were

responsible for the reduction of Fe^{3+} in WSB, causing the discharge of Fe^{2+} and PO_4^{3-} from the reservoir sediments, thus the availability of Fe^{2+}, Mn^{2+}, S^{2-}, and PO_4^{3-} at the WSB.

Estimation of diffusion fluxes of Fe^{2+}, Mn^{2+}, S^{2-}, and PO_4^{3-} at WSB and black water formation in Tianbao reservoir

Diffusion fluxes, measured at the WSB, provide clear understanding of the movement (direction) of elements between the sediment and benthic water (Yuan et al., 2020). In this research work, the fluxes of Fe^{2+}, Mn^{2+}, S^{2-}, and PO_4^{3-} across the WSB in the Tianbao reservoir ranged from 7.4×10^{-5} to 1.3×10^{-4} g/(cm^2 s), 9.2×10^{-6} to 7.9×10^{-5} g/(cm^2 s), -5.4×10^{-7} to 2.2×10^{-7} g/(cm^2 s), and 1.8×10^{-6} to 2.1×10^{-6} g/(cm^2 s), respectively (Fig. 6). It is important to note that positive fluxes show that sediments release metals to the overlying water acting as the source of metal. In contrast, negative fluxes indicate that sediments absorb metals from the overlying water (Wang et al., 2017). From Fig. 6, positive values were observed at all sampling sites for Fe^{2+}, Mn^{2+}, and PO_4^{3-}. The high positive diffusive fluxes recorded in the hypoxic WSB (Fig. 2) indicate that the sediments at the Tianbao reservoir served as a source of Fe, Mn, and P where the sediments release Fe^{2+}, Mn^{2+}, and PO_4^{3-} to the overlying water. For S^{2-}, negative values were observed at A2, A3, and A4, indicating that sediments at these points acted as a sink of S, while sediments at sampling point A1 acted as a source (positive flux value) of S (Fig. 6). The high fluxes of Fe^{2+}, Mn^{2+}, S^{2-}, and PO_4^{3-} played a crucial role in the degradation of the reservoir water by producing black compounds in the benthic water (Fig. S6).

Several research works (Rong et al., 2020) have revealed that water blackening can occur due to the presence of high concentration of ions (Fe^{2+}, Mn^{2+}) and anions (S^{2-}). These ions combine in a favorable redox environment to form black compounds (FeS and MnS, MnS_2). From our research work, a low DO concentration caused changes in the ORP values, creating favorable redox conditions for redox-sensitive metals (Fe^{2+}, Mn^{2+}) to interact with sulfide. In the hypoxic environment, Fe^{2+}, Mn^{2+}, S^{2-}, and PO_4^{3-} are released from sediment pore water to benthic water and easily react

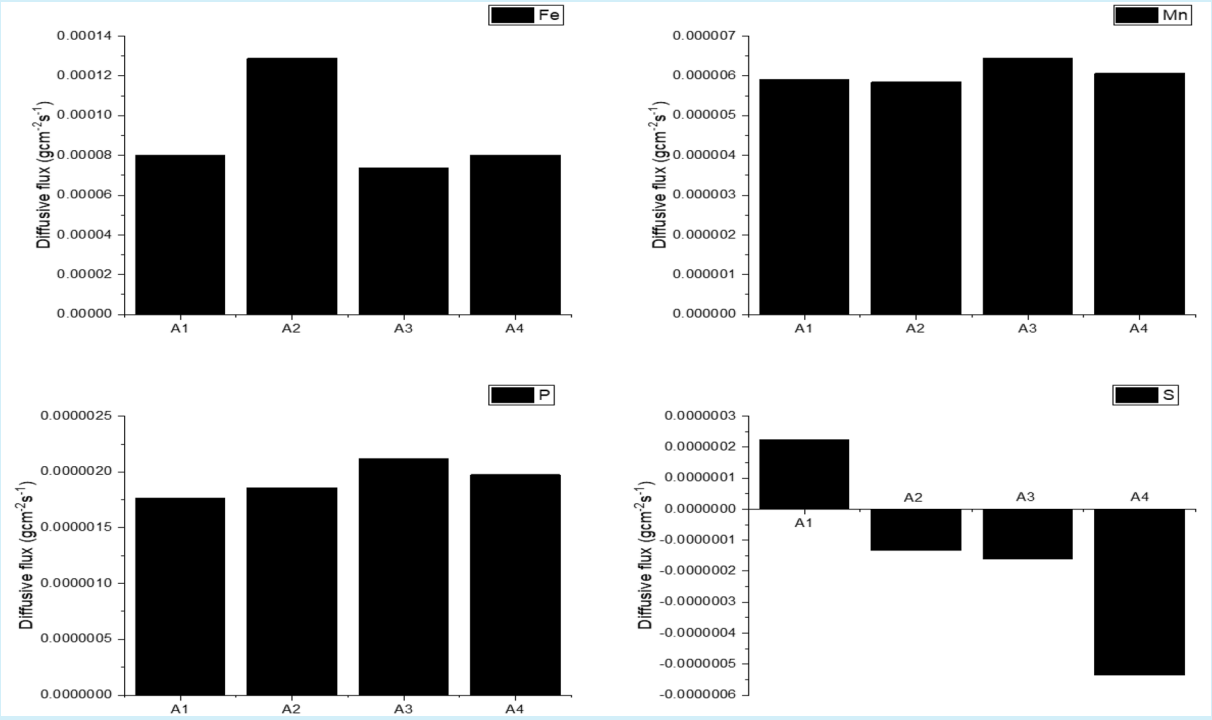

Fig. 6 The fluxes (diffusive) of soluble Fe^{2+}, Mn^{2+}, S^{2-}, and PO_4^{3-} across the water sediment boundary (A1–A4) of the reservoir

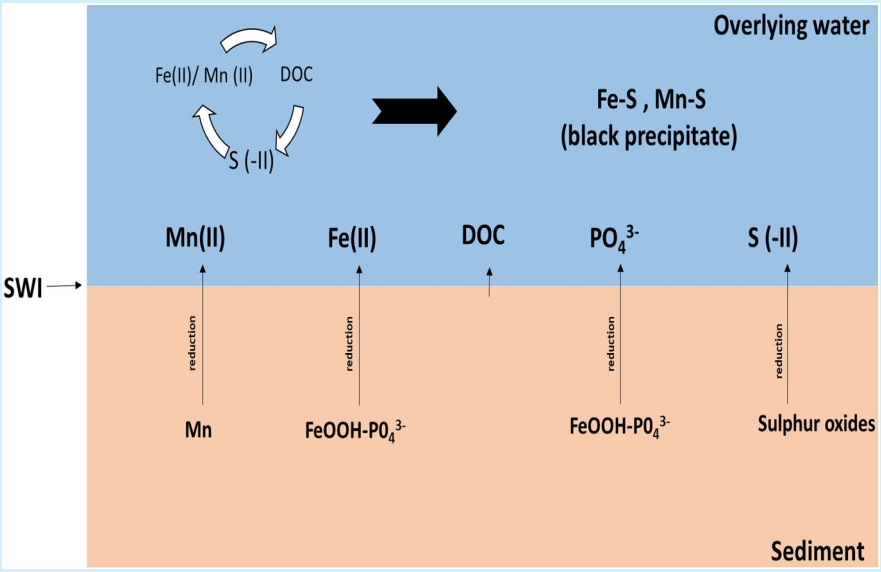

Fig. 7 Description of Fe, P, Mn, and S dynamics at the sediment–water interface (SWI) causing water quality degradation

to form black compounds (Rong et al., 2020). Figure 7 illustrates the schematic description of the mechanism leading to the production of black precipitate at WSB. The sediment which contains FeOOH was the main source of Fe and P for the benthic water (Krueger et al., 2020). In a redox setting, iron-reducing bacteria (IRB) and sulfate-reducing bacteria (SRB) contribute to the transformation of TFe, M, and S in sediments (Zhou et al., 2011). In a water environment with a low ORP value, sulfides are produced, which combine with metallic ions (Fe^{2+}) to form a black precipitate. Other research works have shown that IRB speed up the breakdown and reduction of FeOOH in the sediments, forming Fe^{2+} ions. These ions react with S^{2-} to form black substances (Fig. S6) (Rong et al., 2020). It is worth noting that other metals such as Mn have a low affinity to react with sulfur in a reduced environment; thus, the main cause of the black water event in our study is attributed to Fe (Rong et al., 2020). The results from our study were similar to research works by Luo et al. (2020), where these authors supported the assertion that the sediments with high Fe and Mn content contributed to the formation of black water. These authors explained that these cations have a high affinity to interact with sulfide to form black compounds (i.e., FeS, MnS_2, MnS) forming black water.

Implication of trace metals on the aquatic environment and reservoir water management

Current research works have suggested that investigating black water incidents must not only be done on shallow water bodies (for example, rivers, lakes) but be integrated into reservoirs to safeguard the water quality of reservoirs. Rong et al. (2020) further asserted that at the anoxic WSB, the development of FeS and MnS (black materials) affects aesthetics and water quality. The findings from our study are in line with the above assertions in that it shows the mechanism responsible for the production of black compounds in the reservoirs. The study further shows how human activities (such as manufacture of steel and iron alloys, production of batteries, fireworks, mining activities, and glassware manufacturing) and environmental factors (such as temperature, oxygen distribution-hypoxia, organic matter) affect the production of black materials in the reservoir. These factors are vital in distorting the concentration of Fe^{2+}, Mn^{2+}, S^{2-}, and PO_4^{3-} that negatively affects the reservoir water quality. With the constant development of black materials at the WSB, frequent changes in the physical environment are expected. The reservoir water blackening will greatly reduce natural light penetration into the reservoir, which may affect the well-being of aquatic species in the reservoir. Rong et al.

(2020) revealed that the black water problem affects the aesthetics of water and may cause a water crisis among the inhabitants. We propose that the occurrence of black water must be prevented and the reservoirs should be kept safe from anthropogenic activities as much as possible. Hypoxia is the main driver to the formation of black water. Thus, intervention efforts include the introduction of an air (oxygen) production device to improve the oxygen concentration in the benthic water (Sheng et al., 2013). Another way to address this problem is the addition of chemical oxidants (such as sodium hypochlorite, NaClO; hydrogen peroxide, H_2O_2; potassium permanganate, $KMnO_4$) to WSB to decrease the production of black compound substances (FeS and MnS) (Li et al., 2019a).

Conclusion

In the Tianbao reservoir, southern China, the concentrations of Pb, Cu, Cd, Zn, and Ni based on total risk quotients (TEL and PEL) were investigated. The concentrations of the trace metals in Tianbao sediments were low, suggesting that their harmful impact on the aquatic environment was less. Due to the high concentrations of Fe^{2+}, Mn^{2+}, S^{2-}, PO_4^{3-}, and DOC in the study area, the high-resolution peeper and the DGT technique were used to study their concentration, dynamics, and flux at the WSB. The findings from this study also revealed that the stratification of the Tianbao reservoir occurred for the most of the year except for the winter season (December to February) where mixing of reservoir water occurs. The intense summer stratification of the reservoir, as well as the microbial decomposition of organic matter at the benthic water, intensified the hypoxic conditions at the WSB. Hypoxia was responsible for the high positive flux values of Fe^{2+}, Mn^{2+}, and PO_4^{3-} observed at the WSB. It was suggesting that Fe^{2+}, Mn^{2+}, and PO_4^{3-} move from the sediments into the overlying water. Similarly, the positive and negative flux recorded for S^{2-} suggested that the Tianbao sediments acted as a source or sink of S^{2-}.

The study also showed that the presence of organic matter (TOC) at the WSB was because of the enormous amount of *Eucalyptus* trees around the reservoir. The organic materials from the trees are transported to the reservoir during the harvesting of the trees. Microorganisms use alternate electron acceptors such as Fe^{3+}, Mn^{4+}, and sulfate to an oxidize organic matter under a hypoxic setting and, in the process, convert Fe^{3+}, Mn^{4+}, and sulfate to Fe^{2+}, Mn^{2+}, and S^{2-}, respectively. The reaction of Fe^{2+}, Mn^{2+}, and S^{2-} in the absence of oxygen initiated the production of black precipitate (FeS, MnS, and MnS_2) responsible for the black water occurrence in the reservoir. In short, the use of high-resolution peeper and DGT techniques in the Tianbao reservoir offered a detailed understanding of the dynamics and release risk of Fe^{2+}, Mn^{2+}, S^{2-}, and PO_4^{3-} at WSB affecting water quality and the aquatic environment. The findings of this study serve as a guide and provide valuable knowledge for the public and stakeholders engaged in freshwater quality management designs.

Author contribution Conceptualization: LY; methodology: EN, LY, ZY; formal analysis and investigation: LY, EN, AN; writing — original draft preparation: LY, EN; writing — review and editing: LN; funding acquisition: LY, EN; resources: PY, YH; supervision: RB, DA.

Funding The National Key Research and Development Program of China (2017YFC0405203, 2016YFC0401703) and the National Science Foundation of China (52039003, 51779072, 51809102) supported this research. The Major Science and Technology Program for Water Pollution Control and Treatment (2017ZX07204003) also supported this research.

Availability of data and materials All data generated or analyzed during this study are included in this published article (and its supplementary information files).

Declarations

Conflict of interest The authors declare no competing interests.

References

Akoto, O., Gyimah, E., Zhan, Z., et al. (2019). Evaluation of health risks associated with trace metal exposure in water from the Barekese reservoir in Kumasi, Ghana. *Human and Ecological Risk Assessment: An International Journal,* 7039. https://doi.org/10.1080/10807039.2018.1559033

Battin, T. J. (1998). Dissolved organic matter and its optical properties in a blackwater tributary of the upper Orinoco river, Venezuela. PII S0146–6380(98)00028-X 28:561–569. https://doi.org/10.1002/prop.2190400803

Berthon, J. F., & Zibordi, G. (2010). Optically black waters in the northern Baltic Sea. *Geophysical Research Letters, 37*, 1–6. https://doi.org/10.1029/2010GL043227

Bisutti, I., Hilke, I., & Raessler, M. (2004). Determination of total organic carbon - An overview of current methods. *TrAC Trends in Analytical Chemistry, 23*, 716–726. https://doi.org/10.1016/j.trac.2004.09.003

Cheng, H., Li, K., Li, M., et al. (2014). Geochemical background and baseline value of chemical elements in urban soil in China. *Earth Science Frontiers, 21*, 265–306. https://doi.org/10.13745/j.esf.2014.03.028

Deng, M., Yang, X., Dai, X., et al. (2020). Heavy metal pollution risk assessments and their transportation in sediment and overlay water for the typical Chinese reservoirs. *Ecological Indicators, 112*, 106166. https://doi.org/10.1016/j.ecolind.2020.106166

Duan, H., Ma, R., Loiselle, S. A., et al. (2014). Optical characterization of black water blooms in eutrophic waters. *Science of the Total Environment, 482–483*, 174–183. https://doi.org/10.1016/j.scitotenv.2014.02.113

Duval, B., & Ludlam, S. D. (2001). The black water chemocline of meromictic Lower Mystic Lake, Massachusetts, U.S.A. *International Review of Hydrobiology, 86*, 165–181. https://doi.org/10.1002/1522-2632(200104)86:2%3c165::AID-IROH165%3e3.0.CO;2-Y

He, C., Su, T., Liu, S., et al. (2020). Heavy metal, arsenic, and selenium concentrations in bird feathers from a region in southern China impacted by intensive mining of nonferrous metals. *Environmental Toxicology and Chemistry, 39*, 371–380. https://doi.org/10.1002/etc.4622

Hladyz, S., Watkins, S. C., Whitworth, K. L., & Baldwin, D. S. (2011). Flows and hypoxic blackwater events in managed ephemeral river channels. *Journal of Hydrology, 401*, 117–125. https://doi.org/10.1016/j.jhydrol.2011.02.014

Huang, J., Amuzu-Sefordzi, B., & Li, M. (2015). Heavy metals and polychlorinated biphenyls (PCBs) sedimentation in the Lianhua Mountain Reservoir, Pearl River Delta, China. *Environmental Monitoring and Assessment, 187*, 111–118. https://doi.org/10.1007/s10661-015-4466-x

Huang, J., Norgbey, E., Li, G., et al. (2019). Unraveling the feeding dynamics of Chinese mitten crab-based ecosystems using carbon and nitrogen stable isotope techniques. *Journal of Consumer Protection and Food Safety, 14*(3), 251–261. https://doi.org/10.1007/s00003-019-01220-w

Huang, J., Norgbey, E., Nkrumah, P. N., et al. (2017). Detection of corn oil in adulterated olive and soybean oil by carbon stable isotope analysis. *Journal of Consumer Protection and Food Safety, 12*(3), 201–208. https://doi.org/10.1007/s00003-017-1097-x

Jaishankar, M., Tseten, T., Anbalagan, N., et al. (2014). Toxicity, mechanism and health effects of some heavy metals. *Interdisciplinary Toxicology, 7*, 60–72. https://doi.org/10.2478/intox-2014-0009

Krachler, R., Krachler, R., Valda, A., & Keppler, B. K. (2019). Natural iron fertilization of the coastal ocean by "blackwater rivers." *Science of the Total Environment, 656*, 952–958. https://doi.org/10.1016/j.scitotenv.2018.11.423

Krueger, K. M., Vavrus, C. E., Lofton, M. E., et al. (2020). Iron and manganese fluxes across the sediment-water interface in a drinking water reservoir. *Water Research, 182*, 116003. https://doi.org/10.1016/j.watres.2020.116003

Kummu, M., & Varis, O. (2007). Sediment-related impacts due to upstream reservoir trapping, the Lower Mekong River. *Geomorphology, 85*, 275–293. https://doi.org/10.1016/j.geomorph.2006.03.024

Li, K., Yang, M., Peng, J., et al. (2019a). Rapid control of black and odorous substances from heavily-polluted sediment by oxidation: Efficiency and effects. *Frontiers of Environmental Science & Engineering, 13*(6), 1–11.

Li, R., Wu, Z., Li, L., et al. (2019b). Simulation of fish migration at different water depths based on backpropagation neural network. *Applied Ecology and Environmental Research, 17*, 437–449.

Li, Y., Luo, F., Guo, J., et al. (2018). Mechanism of "blackwater" occurrence in the reservoirs with Eucalyptus plantation, southern China. *Journal of Lake Science, 30*, 15–24. https://doi.org/10.18307/2018.0102

Li, Y., Norgbey, E., Zhu, Y., et al. (2021). Iron, thermal stratification, Eucalyptus sp., and hypoxia: Drivers to water blackening in southern China reservoirs. *Environmental Science and Pollution Research*. https://doi.org/10.1007/s11356-021-12500-0

Li, Y., Nwankwegu, A. S., Huang, Y., et al. (2020). Evaluating the phytoplankton, nitrate, and ammonium interactions during summer bloom in tributary of a subtropical reservoir. *Journal of Environmental Management, 271*, 110971. https://doi.org/10.1016/j.jenvman.2020.110971

Liao, J., Chen, J., Ru, X., et al. (2017). Heavy metals in river surface sediments affected with multiple pollution sources, South China: Distribution, enrichment and source apportionment. *Journal of Geochemical Exploration, 176*, 9–19. https://doi.org/10.1016/j.gexplo.2016.08.013

Liu, M., Zhang, Y., Shi, K., et al. (2019). Thermal stratification dynamics in a large and deep subtropical reservoir revealed by high-frequency buoy data. *Science of the Total Environment, 651*, 614–624. https://doi.org/10.1016/j.scitotenv.2018.09.215

Luo, F., Li, Y., Norgbey, E., et al. (2020). A study on the occurrence of black water in reservoirs in Eucalyptus Plantation region. *Environmental Science and Pollution Research*. https://doi.org/10.1007/s11356-020-09613-3

Marip, J. B., Yuan, X., Zhu, H., et al. (2020). Spatial distribution and environmental significance of phosphorus fractions in river sediments and its influencing factor from hongze and tiaoxi watersheds, Eastern China. *International Journal of Environmental Research and Public Health, 17*, 1–14. https://doi.org/10.3390/ijerph17165787

Marks, B., Peters, A., & McGough, D. (2017). Aquatic environmental risk assessment of manganese processing industries. *Neurotoxicology, 58*, 187–193. https://doi.org/10.1016/J.NEURO.2016.04.011

Melaku, S., Dams, R., & Moens, L. (2005). Determination of trace elements in agricultural soil samples by inductively coupled plasma-mass spectrometry: Microwave acid digestion versus aqua regia extraction. *Analytica Chimica Acta, 543*, 117–123. https://doi.org/10.1016/j.aca.2005.04.055

Murphy, J., & Riley, J. P. (1962). A modified single solution method for the determination of phosphate in natural waters. *Analytica Chimica Acta, 27*, 31–36. https://doi.org/10.1016/S0003-2670(00)88444-5

Norgbey, E., Huang, J., Hirsch, V., et al. (2020a). Unravelling the efficient use of waste lignin as a bitumen modifier for sustainable roads. *Construction and Building Materials, 230*, 116957. https://doi.org/10.1016/j.conbuildmat.2019.116957

Norgbey, E., Li, Y., Ya, Z., et al. (2020b). High resolution evidence of iron-phosphorus-sulfur mobility at hypoxic sediment water interface: An insight to phosphorus remobilization using DGT-induced fluxes in sediments model. *Science of the Total Environment, 724*, 138204. https://doi.org/10.1016/j.scitotenv.2020.138204

Norgbey, E., Li, Y., Zhu, Y., et al. (2021). Seasonal dynamics of iron and phosphorus in reservoir sediments in Eucalyptus plantation region. *Ecological Processes, 10*.https://doi.org/10.1186/s13717-021-00280-x

Nwankwegu, A. S., Li, Y., Huang, Y., et al. (2020a). Nitrate repletion during spring bloom intensifies phytoplankton iron demand in Yangtze River tributary, China. *Environmental Pollution, 264*, 114626. https://doi.org/10.1016/j.envpol.2020.114626

Nwankwegu, A. S., Li, Y., Huang, Y., et al. (2020b). Nutrient addition bioassay and phytoplankton community structure monitored during autumn in Xiangxi Bay of Three Gorges Reservoir, China. *Chemosphere, 247*, 125960. https://doi.org/10.1016/j.chemosphere.2020.125960

Rong, N., Lu, W., Zhang, C., et al. (2020). In situ high-resolution measurement of phosphorus, iron and sulfur by diffusive gradients in thin films in sediments of black-odorous rivers in the Pearl River Delta region, South China. *Environmental Research*, *189*.https://doi.org/10.1016/j.envres.2020.109918

Shao, Y., Chen, Z., & Wu, L. (2019). Oxidative stress effects of soluble sulfide on human hepatocyte cell line lo2. *International Journal of Environmental Research and Public Health*, *16*. https://doi.org/10.3390/ijerph16091662

Sheng, Y., Qu, Y., Ding, C., et al. (2013). A combined application of different engineering and biological techniques to remediate a heavily polluted river. *Ecological Engineering, 57*, 1–7. https://doi.org/10.1016/j.ecoleng.2013.04.004

Shyla, B., Mahadevaiah, & Nagendrappa, G. (2011). A simple spectrophotometric method for the determination of phosphate in soil, detergents, water, bone and food samples through the formation of phosphomolybdate complex followed by its reduction with thiourea. *Spectrochimica Acta Part A: Molecular and Biomolecular Spectroscopy, 78*, 497–502. https://doi.org/10.1016/j.saa.2010.11.017

Soto-Neira, J., Zhu, Q., & Aller, R. C. (2011). A new spectrophotometric method to quantify dissolved manganese in marine pore waters. *Marine Chemistry, 127*, 56–63. https://doi.org/10.1016/j.marchem.2011.07.009

Tamura, H., Goto, K., Yotsuyanagi, T., & Nagayama, M. (1974). Spectrophotometric determination of iron(II) with 1,10-phenanthroline in the presence of large amounts of iron(III). *Talanta, 21*, 314–318. https://doi.org/10.1016/0039-9140(74)80012-3

Tue-Ngeun, O., Sandford, R. C., Jakmunee, J., et al. (2005). Determination of dissolved inorganic carbon (DIC) and dissolved organic carbon (DOC) in freshwaters by sequential injection spectrophotometry with on-line UV photo-oxidation. *Analytica Chimica Acta, 554*, 17–24. https://doi.org/10.1016/j.aca.2005.08.043

Valett, H. M., Baker, M. A., Morrice, J. A., et al. (2005). Biogeochemical and metabolic responses to the flood pulse in a semiarid floodplain. *Ecology, 86*, 220–234. https://doi.org/10.1890/03-4091

Wang, Y., Ding, S., Shi, L., et al. (2017). Simultaneous measurements of cations and anions using diffusive gradients in thin films with a ZrO-Chelex mixed binding layer. *Analytica Chimica Acta, 972*, 1–11. https://doi.org/10.1016/j.aca.2017.04.007

Whitworth, K. L., & Baldwin, D. S. (2016). Improving our capacity to manage hypoxic blackwater events in lowland rivers: The blackwater risk assessment tool. *Ecological Modelling, 320*, 292–298. https://doi.org/10.1016/j.ecolmodel.2015.10.001

Whitworth, K. L., Kerr, J. L., Mosley, L. M., et al. (2013). Options for managing hypoxic blackwater in river systems: Case studies and framework. *Environmental Management, 52*, 837–850. https://doi.org/10.1007/s00267-013-0130-9

Xu, D., Wu, W., Ding, S., et al. (2012). A high-resolution dialysis technique for rapid determination of dissolved reactive phosphate and ferrous iron in pore water of sediments. *Science of the Total Environment, 421–422*, 245–252. https://doi.org/10.1016/j.scitotenv.2012.01.062

Yan, R., Gao, Y., Li, L., & Gao, J. (2019). Estimation of water environmental capacity and pollution load reduction for urban lakeside of Lake Taihu, eastern China. *Ecological Engineering, 139*, 105587. https://doi.org/10.1016/J.ECOLENG.2019.105587

Yuan, H., Tai, Z., Li, Q., & Liu, E. (2020). In-situ, high-resolution evidence from water-sediment interface for significant role of iron bound phosphorus in eutrophic lake. *Science of the Total Environment, 706*, 136040. https://doi.org/10.1016/j.scitotenv.2019.136040

Zhang, Y., Han, Y., Yang, J., et al. (2017). Toxicities and risk assessment of heavy metals in sediments of Taihu Lake, China, based on sediment quality guidelines. *Journal of Environmental Sciences (China), 62*, 31–38. https://doi.org/10.1016/j.jes.2017.08.002

Zhang, Y., Yang, J., Simpson, S. L., et al. (2019). Application of diffusive gradients in thin films (DGT) and simultaneously extracted metals (SEM) for evaluating bioavailability of metal contaminants in the sediments of Taihu Lake, China. *Ecotoxicology and Environmental Safety, 184*, 109627. https://doi.org/10.1016/j.ecoenv.2019.109627

Zhang, Z., Cao, R., Mamat, Z., et al. (2020). A study of synchronous measurement of liable phosphorous and iron based on ZrO-Chelex (DGT) in the sediment of the Chaiwopu Lake, Xinjiang, Northwest China. *Environmental Science and Pollution Research, 27*, 15057–15067. https://doi.org/10.1007/s11356-020-07701-y

Zhou, J., He, Q., Hemme, C. L., et al. (2011). How sulphate-reducing microorganisms cope with stress: Lessons from systems biology. *Nature Reviews Microbiology, 9*, 452–466.

Zhuang, W., Ying, S. C., Frie, A. L., et al. (2019). Distribution, pollution status, and source apportionment of trace metals in lake sediments under the influence of the South-to-North Water Transfer Project, China. *Science of the Total Environment, 671*, 108–118. https://doi.org/10.1016/j.scitotenv.2019.03.306